

Stochastic Spreading of Intracellular Ca^{2+} Release

Martin Falcke¹, Lev Tsimring², and Herbert Levine¹

¹*University of California San Diego, Physics Department
9500 Gilman Drive La Jolla, CA, 92093-0319*

²*University of California San Diego,
Institute for Nonlinear Science
9500 Gilman Drive La Jolla, CA, 92093-0402*

(May 10, 2000)

We study the spreading of Calcium Induced Calcium Release with the stochastic DeYoung-Keizer-model of the inositol 1,4,5-trisphosphate receptor channel. The model shows a transition from isolated release events to steadily propagating waves with increasing IP_3 concentration. A new state - stochastic backfiring - was found in the regime of steady propagation. The model can be reduced by an adiabatic elimination of the partial differential equation for the Ca^{2+} concentration to a lattice of stochastic channel clusters.

PACS: 87.16.Xa, 05.40.-a, 82.20.Mj

I. INTRODUCTION

Calcium often acts as a second messenger in living cells so as to regulate multiple cellular functions. These functions include processes as diverse as muscle contraction and synaptic transmission [1,2]. The Ca^{2+} signal initially employed in these processes consists of a transient increase in the intracellular concentration. This increase can arise from influx through the cell membrane or via Ca^{2+} release from internal stores. The release from internal stores like the endoplasmic reticulum is a nonlinear process, since calcium induces its own further release. That allows for the formation of complex spatio-temporal signals in form of localized stochastic release events (puffs, sparks) or waves of high Ca^{2+} concentration traveling across the cell.

Intracellular calcium waves were first observed in medaka eggs [3] and later on in e.g. *Xenopus* oocytes [4,5], hepatocytes [6], articular chondrocytes [7] and cardiac myocytes [8,9]. Puffs have been observed in *Xenopus* oocytes, skeletal muscle cells, and heart muscle cells [10–16]. Most relevant for our work, Parker et al. [14] showed for a single cell type, (the *Xenopus* oocyte), there exists a continuum of wave phenomena. At low excitability, isolated puffs are observed. Abortive waves occur at higher excitability and a further increase of excitability leads to steadily propagating waves.

Ca^{2+} is released from the endoplasmic reticulum through channels. As we have already mentioned, this process is nonlinear since as a general pattern, increased Ca^{2+} concentration in the cytosol favors channel opening. This autocatalytic amplification is called Calcium Induced Calcium Release CICR. There are a variety of channels showing CICR. Here, we will focus on the inositol 1,4,5-trisphosphate receptor channel IP_3R . This channel consists of four identical subunits. Each subunit has an activating binding site for IP_3 , an activating site for Ca^{2+} and an inhibiting Ca^{2+} binding site. Experi-

mental findings suggest that the channel is open if both Ca^{2+} and IP_3 are bound to the activating sites and at the same time Ca^{2+} is not bound to the inhibiting site, at least three out of the four subunits. Binding of Ca^{2+} to the inhibiting site of one of these subunits closes the channel. It can reopen after dissociation of Ca^{2+} from the inhibiting sites. The bindings of Ca^{2+} to the activating and inhibiting sites are stochastic events rendering the opening and closing of the channel a stochastic process.

There is a vast literature devoted to intracellular Ca^{2+} waves approximating the Ca^{2+} channels as a deterministic and spatially continuous source term [17–21,23–25]. These reaction-diffusion models explain the observed wave patterns as nonlinear waves in (depending on model parameters) an excitable, oscillatory or bistable medium. Extensions to these models which include the fact that the channels act as discrete Ca^{2+} sources elucidate the transition from localized to traveling structures [26–28]. However, the observation of localized stochastic Ca^{2+} puffs and the rather small number of channels creating the localized event suggest that stochastic effects are relevant for Ca^{2+} wave propagation and need to be taken into account when waves are modeled mathematically. Indeed, abortive waves cannot be understood in terms of deterministic models, since in these models an excitation travels steadily if it travels at all.

More recently, Keizer et al. [29,30] introduced a stochastic, spatially discrete model for waves in cardiac myocytes. Using direct stochastic simulations, this group demonstrated the existence of a spark to wave transition. In this work, the dynamics of the ryanodine receptor channel is treated as a stochastic process, coupled to the evolution of the spatial profile of the Ca^{2+} concentration which is modeled by a reaction diffusion equation. In section II, we will present an analogous model for the IP_3R system. It is based on the DeYoung-Keizer-model [31,32] for the channel kinetics of the IP_3 receptor channel. Some

simulations of this model, demonstrating the transitions from spark to abortive wave to steady wave, are shown in sec. III. Also, we find a new "back-firing" state which is due to the stochasticity in the channel dynamics. This state appears to be consistent with experimental findings where persistent wave activity was observed in a regime where spiral waves do not exist [21,22].

Next, we present a more general approach to the mathematical modeling of discrete, active elements coupled by fast diffusion. In the paradigm used to date, the channels can be perceived as a array of stochastic elements coupled by the Ca^{2+} concentration field $c(\mathbf{r},t)$ (\mathbf{r} and t denote the spatial and time coordinate resp.). The state of the complete system is determined by the states of all channel subunits at the current time and $c(\mathbf{r},t)$. The Ca^{2+} concentration affects the transition probabilities between different states for the individual subunits and thereby couples channels by diffusion. We will argue that it is reasonable to assume that the concentration profile evolves on a time scale much faster than that of the channel dynamics and in fact merely exhibits relaxation dynamics to an asymptotic state, as long as the channel configuration remains unchanged. Then, one can ignore this transient period and use instead the time independent transition rates derivable from the asymptotic state of the concentration profile for the actual configuration of channel states. This then reduces the complete model to a Markov process in the channel configuration space alone. We will present this approach in Sec. IV and derive a reduced IP_3R model.

In section V, we compare the results of simulating the original model and the reduced one. Our results indicate that one can in fact recover the correct dynamics in a reasonably quantitative manner. In particular, the aforementioned backfiring state is obtained in the reduced model. Finally, we summarize our results in a brief concluding section.

II. THE MODEL

In this section, we introduce a model describing the intracellular calcium dynamics arising via diffusion and via the IP_3 receptor. It has been observed experimentally [11] that the channels are spatially organized in clusters. We therefore consider a regular array of channel clusters with spacing d and with N_K channels per cluster. In most calculations the cluster radius R was fixed to be $0.225 \mu\text{m}$. That size can accommodate up to 40 channels. We do not spatially resolve the location of individual channels inside a cluster. These clusters interact with the Ca^{2+} in two ways. First, the open channels act as calcium sources. Second, the transition rates between different channel states are calcium dependent. We describe each of these effects in turn.

The dynamics of $[\text{Ca}^{2+}]$ - denoted c - is modeled by a diffusion equation with spatially discrete source terms corresponding to the clusters. Let us define the maximum flux coefficient J_K to be the coefficient relating calcium flux to concentration difference (across the ER membrane) if channels are open. Then, the actual calcium release flux for the i th cluster is given by $\alpha(J_L + (N_o^i/N_K)J_K)(c_{ER} - c)$ with c_{ER} denoting the Ca^{2+} concentration in the endoplasmic reticulum, α the ratio of ER volume to cell volume, and N_o^i denotes the number of open channels. The constant J_L determines the leak flux. Following Keizer et al. [29,32], we approximate c_{ER} by the local condition $\alpha c_{ER} + c = C_o$ with C_o constant; this guarantees the conservation of the total Ca^{2+} content of the (closed) cell.

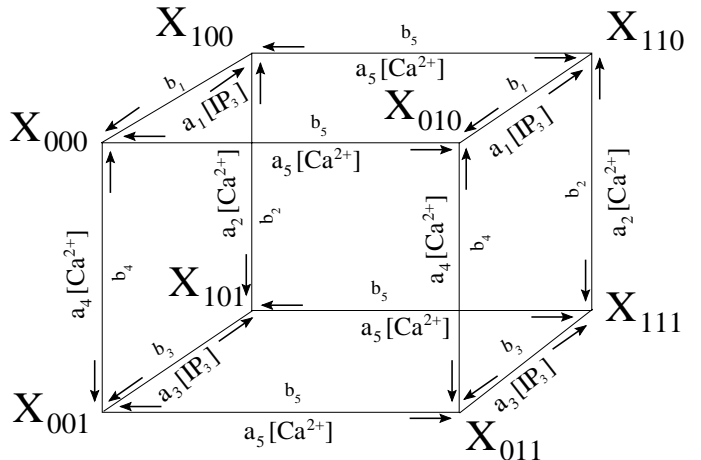


FIG. 1. States X_{ijk} of a subunit of the IP_3 receptor channel. An index is 1 if an ion is bound and 0 if not. The index i stands for the IP_3 site, j for the activating Ca^{2+} site and k for the inhibiting Ca^{2+} site. The transition rates are given at the edges of the cube.

In addition, Ca^{2+} is removed from the cytosol back into the endoplasmic reticulum by SERCATPases pumping against the concentration gradient. We model this flux by a term J_{PC} . It would be more realistically modeled by a second order Hill dynamics but was approximated by a linear dependence on c for the sake of obtaining an analytic solution of the diffusion equation (see below). We assume that there is no room for SERCA's inside channel clusters and that they are distributed uniformly outside clusters. Hence Ca^{2+} is pumped back into the ER only in regions outside of clusters, with a spatially continuous flux density. Denoting the Ca^{2+} diffusion coefficient D and the cluster locations \mathbf{R}_i , we obtain a pair of coupled equations for the Ca^{2+} profile inside a cluster c_{in} and outside c_{out} :

$$\frac{\partial c_{in}}{\partial t} = D \frac{\partial^2 c_{in}}{\partial r^2} + (1 + \alpha)(J_L + \frac{N_o^i}{N_K} J_K) (\frac{C_o}{1 + \alpha} - c_{in}) \quad (1)$$

$$|\vec{r} - \vec{R}_i| \leq R$$

$$\frac{\partial c_{out}}{\partial t} = D \frac{\partial^2 c_{out}}{\partial r^2} + (1 + \alpha) J_L \left(\frac{C_o}{1 + \alpha} - c_{out} \right) - J_P c_{out} \quad (2)$$

$$\left| \vec{r} - \vec{R}_i \right| \geq R$$

TABLE I. Parameters of the model. The parameters of receptor binding and dissociation are taken from [31].

Next, we discuss the role of calcium in regulating the transition rates between the different possible states of the channel. We adopt the DeYoung-Keizer-model for the IP₃ receptor channel [31,32]. The three binding sites on each subunit allow for 8 different states X_{ijk} for each subunit. The index i stands for the IP₃ site, j for the activating Ca²⁺ site and k for the inhibiting Ca²⁺ site (see Fig.1). An index is 1 if an ion is bound and 0 if not. The transition rates between the states X_{0jk} and X_{1jk} (IP₃ binding and dissociation) are two orders of magnitude faster than the other transition rates (see Table I). Therefore we assume these pairs of states to equilibrate immediately and lump them into single states X_{jk} = X_{0jk} + X_{1jk}. The kinetic scheme then reduces to the one shown in Fig.2. The state with no Ca²⁺ ion bound is X₀₀, the activated state is X₁₀ and the inhibited states are X₁₁ and X₀₁.

We have already mentioned that a channel consists of four subunits, of which three have to be activated for the channel to open. However, DeYoung and Keizer in their original paper derived expressions for the opening probability of a channel based on the

Par.	Description	Value
<u>Ca²⁺</u>		
J _L	Leak current	0.05 s ⁻¹
J _K	Current per cluster	varies
J _P	Pump capacity	varies
α	volume endopl.ret./volume cell	0.185
C _o	total [Ca ²⁺]	varies
I	[IP ₃]	varies
I _b	$\frac{I}{I+d_1}$	varies
N _K	number of channels per cluster	varies
N _o ⁱ	number of open channels of the ith cluster	varies
D	Ca ²⁺ diffusion coefficient	30 μm ² s ⁻¹
<u>receptor binding</u>		
a ₁	IP ₃	400 μM ⁻¹ s ⁻¹
a ₂	Ca ²⁺ , inhibiting site	0.2 μM ⁻¹ s ⁻¹
a ₃	IP ₃	400 μM ⁻¹ s ⁻¹
a ₄	Ca ²⁺ , inhibiting site	0.2 μM ⁻¹ s ⁻¹
a ₅	Ca ²⁺ , activating site	20 μM ⁻¹ s ⁻¹
a ₆	$\frac{a_2 I}{I+d_1} + \frac{d_1 a_4}{I+d_1}$	0.2 μM ⁻¹ s ⁻¹
<u>receptor dissociation d_i=b_i/a_i, i=1-5</u>		
d ₁	IP ₃	0.13 μM
d ₂	Ca ²⁺ , inhibiting site	1.049 μM
d ₃	IP ₃	0.9434 μM
d ₄	Ca ²⁺ , inhibiting site	0.1445 μM
d ₅	Ca ²⁺ , activating site	0.08234 μM
b ₆	$\frac{b_2 I}{I+d_3} + \frac{d_3 b_4}{I+d_3}$	varies

(inaccurate) assumption that three out of three subunits are in the state X_{110} [31]. For our initial investigation, we decided to stick to this approach, thereby allowing us to use their parameters (given in the table); calculations which assume that a channel opens when three out of four subunits are in X_{110} will be reported in the future.

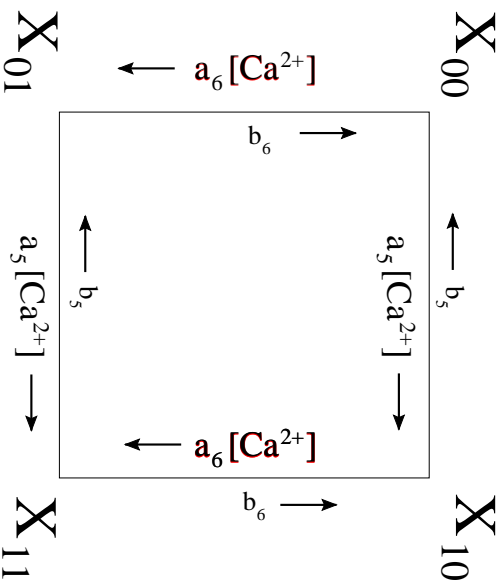


FIG. 2. Lumped states X_{j_k} of a subunit of the IP_3 receptor channel. An index is 1 if an ion is bound and 0 if not. The index j stands for the activating Ca^{2+} site and k for the inhibiting Ca^{2+} site. The transition rates are given at the edges of the rectangle.

III. SIMULATIONS

We perform simulations of the complete model by integrating equations (1,2) with the actual configuration of open channels $N_o^i(t)$, the value of which is obtained from stochastic simulations of the channel dynamics with $c(r,t)$. The initial state for the Ca^{2+} concentration was always $c(r,0)=C_s$ (see equ.(A7)). For all parameter values used in this paper, C_s is very small, leading to the initial state (0,0) for the channel subunits. For the stochastic part of the simulation, each subunit was independently updated. For this model, there are two possible transitions out of each subunit state, with transition probabilities (rates multiplied by the time-step of typically $5 \cdot 10^{-4}s$) p_i and p_j . A random number ρ between 0 and 1 was drawn from a uniform distribution for each update step. The subunit was set to state i if $\rho \leq p_i$, to state j if $p_i < \rho \leq p_i+p_j$ and remained in its current state otherwise. Subunits in X_{10} are in the activated substrate X_{110} with the conditional probability I_b (see Table I) that IP_3 is bound, given the state X_{10} .

Experiments show that the spatio-temporal patterns of calcium in *Xenopus oocytes* change from isolated puffs at low $[IP_3]$, to abortive waves at intermediate $[IP_3]$ and finally steady waves. Our model reproduces this basic finding, as shown in Fig.3. The transition can be

explained by the increase in IP_3 binding probability with increasing $[IP_3]$ and hence an increased fraction of the state X_{110} of the lumped state X_{10} . Additionally, inhibition decreases with increasing $[IP_3]$.

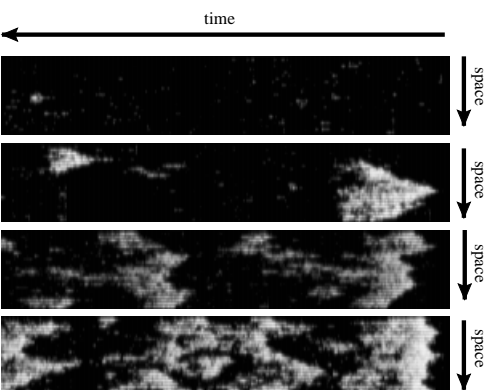


FIG. 3. Spontaneous wave patterns in one spatial dimension for different $[IP_3]$ from left to right: $0.25 \mu M$, $0.3 \mu M$, $0.4 \mu M$ and $0.5 \mu M$. Bright gray levels indicate high Ca^{2+} concentration. Spontaneous, isolated sparks occur for $I=0.25 \mu M$. At $I=0.3 \mu M$, abortive waves appear. The waves at $I=0.4 \mu M$ and $I=0.5 \mu M$ no longer die out but instead disappear at the boundary or by collision. Parameters not given in Table I are $J_P=20 \mu M s^{-1}$, $J_K=135 s^{-1}$, $J_I=0.2 s^{-1}$, $d=2.4 \mu m$, $C_o=1.5 \mu M$, $N_K=20$. The time interval shown is $625s$ and the spatial extension is $600 \mu m$.

Simulations of this system also lead to a new type of spatio-temporal pattern, that is characterized by backfiring. Here, propagating pulses can lead to the creation (in their wake) of oppositely propagating pulses (in one dimension) or of new signaling centers (in higher dimension). A typical picture in two dimensions is shown in Fig. 4*. One interesting new possibility concerns the formation of a spatio-temporally disordered calcium concentration pattern, as shown for example in Fig. 5. This simulation shows that there is no need for pacemakers to generate continuing wave patterns which are not spirals. In fact, once a single channel opens spontaneously, the wave activity can sustain itself via backfiring. We will return to a further discussion of backfiring after we discuss the idea of reduced modeling based on adiabatic elimination of the calcium concentration field.

*The values of J_K used in the simulation may seem large compared to continuous models. However, values in this order of magnitude arise naturally by concentrating the flux in a volume $R^2 d$.

IV. REDUCTION OF THE MODEL

Our complete model, as derived in the previous section, consists of a partial differential equation eqn.(1,2) for c and a stochastic scheme for the set of subunits. In this section, we discuss an approximation in which the calcium dynamics is adiabatically eliminated so as to obtain a stochastic Markov process for the channel configurations alone. This elimination can be justified by a comparison of the time scales of the Ca^{2+} dynamics and the channel dynamics. The diffusion time for a distance of the cluster spacing d and the rise time for Ca^{2+} after channel opening are both of order 0.1s or faster. On the other hand, time scales for the channel dynamics are perhaps 1s or longer. In ref. [33], we used this notion to motivate the study of a (postulated) stochastic channel model; here, we show how this type of model can be derived in detail.

To proceed, we introduce the activation probability for a given subunit j as $p^+(j, \{N_o\})$; this probability depends on the set of N_o^i , the entire configuration vector of the number of open channels in each of the N_{cl} clusters, $i=1, \dots, N_{cl}$. There is a similar probability for subunit inhibition, which we denote as p^- . These probabilities depend on the calcium concentration at position R_j . In our adiabatic elimination scheme, we calculate this concentration by solving the

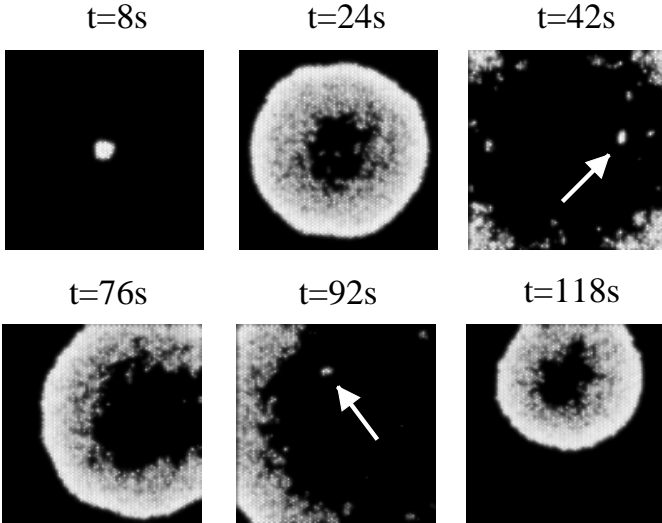


FIG. 4. Backfiring in two spatial dimensions. Bright gray levels indicate high Ca^{2+} concentration. An expanding ring emerges from an initial puff. It leaves behind small excited patches. Some of them (white arrows) set off another wave. Shown is an area of $96\mu\text{m} \times 96\mu\text{m}$. Parameters other than those given in Table I are $I=0.17 \mu\text{M}$, $J_P=57.14 \mu\text{M}\text{s}^{-1}$, $J_K=4500 \text{ s}^{-1}$, $J_L=0.05 \text{ s}^{-1}$, $d=1.5 \mu\text{m}$ on a hexagonal grid, $C_o=0.7 \mu\text{M}$, $N_K=56$, $d_2=1.193 \mu\text{M}$, $d_3=0.9437 \mu\text{M}$, $d_4=0.164\mu\text{M}$, $R=0.2\mu\text{m}$. Numerical parameters: Crank-Nicholson alternating direction scheme, spatial discretization $0.1 \mu\text{m}$, time discretization 0.001s .

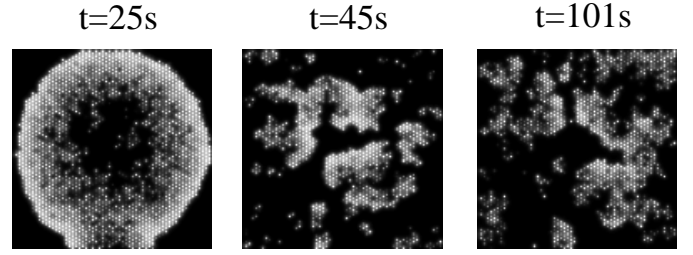


FIG. 5. Turbulent backfiring in two spatial dimensions. Bright gray levels indicate high Ca^{2+} concentration. The initial wave leaves behind a turbulent state with wave fragments traveling in an irregular manner. Shown is an area of $96\mu\text{m} \times 96\mu\text{m}$. Parameters different from those in Table I are $I=0.25 \mu\text{M}$, $J_P=50 \mu\text{M}\text{s}^{-1}$, $J_K=3610 \text{ s}^{-1}$, $J_L=0.05 \text{ s}^{-1}$, $d=1.9\mu\text{m}$ on a hexagonal grid, $C_o=0.8 \mu\text{M}$, $N_K=42$, $R=0.2\mu\text{m}$. The numerical parameters are the same as in the preceding figure.

steady-state calcium reaction-diffusion equation that results from having these open channels. In Appendix A, the concentration profile is derived for two simple cases, that of a single open cluster of channels and that of a periodic array of open clusters. For the former, the full solution exhibiting the rate of approach to the steady-state is also obtained. The single cluster situation is what might be typical of a system exhibiting isolated puffs.

Note that the remaining processes, that of de-inhibition and de-activation, are calcium independent. If the rates are denoted respectively as b_5 and b_6 , the probabilities are obtained merely by multiplying these by the time-step dt . We append to all these transition probabilities the method introduced in the previous section to determine the number of open channels given the number of activated subunits. We have thereby defined a stochastic process for channel sub-unit dynamics.

Rather than study this complex Markov process, we will actually make an additional approximation. It is clearly the case that the most important contributors to the calcium concentration at cluster j are the nearby open channels. We will therefore make a local approximation in which the dependence of $c(R_j, \{N_o\})$ on the overall set of open channels is replaced by a dependence on the number of open channels at a small number of nearby sites, j and $j \pm i, i \leq 4$. Furthermore, we will approximate the full dependence of the calcium concentration on the channel variables as a sum of terms that depend separately on the number of open channels at each site i.e. terms of the form (A15,A16) in one spatial dimension and (A17,A18) in two dimensions both taken at $t=\infty$. We have checked that this linear approximation is quantitatively valid as long as the channel spacing is large enough. We do not as yet linearize the dependence on the number of open channels at each site; we will see later that this too is possible if one merely wishes to obtain qualitative insight.

Thus, our basic model takes the form

$$p^+(j, \{N_o\}) = a_5 dt \sum_{i=-4}^4 c_s(R_j + id; N_o^{i+j}) \quad (3)$$

Here, c_s is the stationary concentration profile for N_o open channels; the calculation of this object is discussed in Appendix A. We have an analogous expression for $p^-(j, \{N_o\})$ which now involves a_6 . In Fig. 6, we show the dependence of the activation probability on the number of open channels for the on-site term in eq. 3 and for the next nearest neighbor term as well. Finally, a channel was considered to be open with the probability I_b^3 that IP_3 is bound to all three subunits (see Table I) if all three subunits were in the state (10)

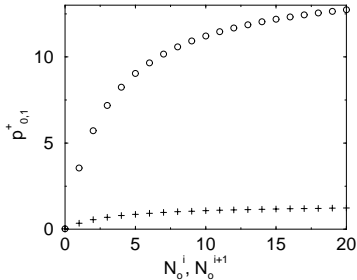


FIG. 6. The transition rates for on-site p_0^+ and neighboring site p_1^+ open channels N_o . Parameters not given in Table I are $d=2\mu\text{m}$, $J_P=52.5 \mu\text{M s}^{-1}$, $N_K=20$, $J_K=1100 \text{ s}^{-1}$, $J_L=0.05 \text{ s}^{-1}$, $C_o=0.8 \mu\text{M}$, $R=0.2\mu\text{m}$.

The calcium response curve in the figure just discussed is clearly nonlinear. Note especially that there is a saturation effect in how the on-site probability responds to increasing numbers of open channels. Nevertheless, we might consider taking the reduction a step further and treat the dependence of p^+ and p^- on N_o^i as a linear relation. Specifically, we define the slopes $\ell^\pm = g(p^\pm(N_K) - p^\pm(0))/N_K$, with g a fitting parameter that this be $O(1)$. Note that all the various probabilities (on-site versus displaced, activation versus inhibition) are chosen to have the same coefficient g , so as to ensure that the ratios of our probabilities remain N_o independent. Furthermore we simplified the calculation of the number of open channels from the number of activated subunits. Instead of keeping track of each channel separately, we use the approximation that the number of open channels can be determined from the number m_{10} of subunits in the state (10) via the relation $N_o = m_{10}^3/(9N_K^2)$; this is easily shown to be the expected number of open channels for large enough N_k . Aside from the (weak) dependence on sites more distant than the nearest neighbor clusters, this final reduced model is essentially the same as the phenomenological model which we have recently introduced in ref. [33].

V. REDUCED MODEL SIMULATION RESULTS

In the last section, we have defined two stages of reduced models, the difference being essentially whether or not we linearize the calcium response curve. Simulations were done in a similar manner to those already discussed for the full model. We did test the sensitivity of our results to the time-step (using time intervals of $5 \cdot 10^{-3}\text{s}$ or 10^{-2}s); we did not observe any noticeable differences.

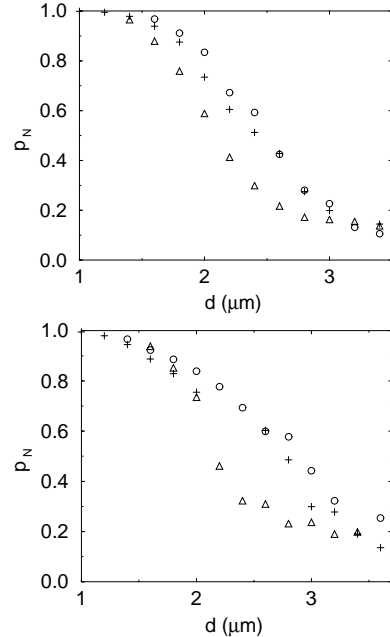


FIG. 7. The probability p_N that an active cluster activates a neighboring cluster in dependence on the cluster spacing d for the different models. The flux density ((single channel flux)/ d) was kept constant by multiplying J_K for $d=1\mu$ with d . The values for J_K given below are those used for $d=1\mu$. Parameters not given in Table I are $[IP_3]=0.34 \mu\text{M}$, $J_L=0.05 \text{ s}^{-1}$, $C_o=0.85 \mu\text{M}$, top: $J_P=50 \mu\text{Ms}^{-1}$, $J_K=350 \text{ s}^{-1}$, $N_K=20$; bottom: $J_P=28.23 \mu\text{Ms}^{-1}$, $J_K=210 \text{ s}^{-1}$, $N_K=12$. The line styles are: complete model \circ , reduced model $+$, reduced model with linearized transition rates Δ . The slope parameter g is 1.3 (top) and 1.0 (bottom).

The first issue we wish to address concerns the transition from localized to propagating disturbances. Propagation can be characterized by the probability p_N that an active cluster activates a neighboring cluster. It can be obtained from the probability $S(i)$ that an initial excitation travels at least up to the i th cluster: $S(i) \sim p_N^i$. p_N increases smoothly from 0 to 1 as we increase the coupling between clusters, increase the lifetime of the activated state of a cluster or increase the number of channels per cluster. Fig.7 shows simulation results for the complete model and both reductions. The results agree very well and clearly indicate that the Ca^{2+} dynamics can be adiabatically eliminated. For the reduced model

with linearized transition rates that agreement was used after fitting g ; note though that the same value of g was used for all channel spacings.

There is quantitative agreement of the results obtained with the reduced model with the results of the complete model. The p_N calculated with the reduced model with linearized transition rates fall faster with increasing d than the probabilities obtained with the other two models. However, this difference does not arise from the adiabatic elimination of the Ca^{2+} dynamics but rather from the linearization or the approximation used to calculate the number of open channels from the number of active subunits.

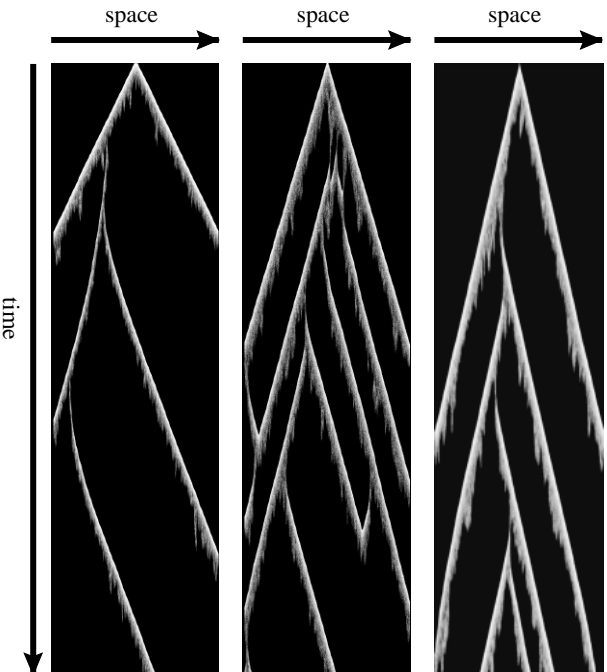


FIG. 8. Traveling pulse emitting pulses backwards (backfiring) with the complete model (top, $J_P=52.5 \mu\text{M s}^{-1}$), the reduced model (middle, $J_P=46.25 \mu\text{M s}^{-1}$) and the reduced model with linearized transition rates (bottom, $J_P=46.25 \mu\text{M s}^{-1}$, $g=1.8$). Bright gray levels indicate large numbers of open channels. Further parameters not given in Table I are $J_K=528 \text{ s}^{-1}$, $I=0.34 \mu\text{M}$, $J_I=0.05 \text{ s}^{-1}$, $d=1.5 \mu\text{m}$, $C_o=0.8 \mu\text{M}$, $N_K=250$. The time interval shown is 234s and the spatial extension is $600 \mu\text{m}$. For the complete model, we show the Ca^{2+} concentration (increasing with the brightness). The fraction of open channels is shown for the reduced models. As can be seen in the middle panel of Fig.8, one wave might survive the collision of two waves in the backfiring regime. That is true for the complete linearized model too.

Recall that in the full simulation, a new state was observed within the regime of steady propagation. This new state is formed when traveling pulses emit new pulses which travel backward - opposite to its direction of propagation. The emitted pulses are initiated by active channels in the refractory tail of the original pulse. There are in principle two ways in which channels can be activated there; it is possible that they were originally acti-

vated by the first pulse and have not as yet become inhibited or alternatively they may have already undergone the complete activation-inhibition-deinhibition cycle and hence can be re-opened. We always found the latter scenario to be the case for the sample clusters which we looked at in more detail during our simulations. Note that the Ca^{2+} level in the refractory area is less than in the excited region but higher than the base level. This provides an increased opening-probability as compared to the medium in front of the pulse. If a group of re-opened channels stays open long enough for sufficient decay of the inhibition around it, it can set off another wave.

We found backfiring at intermediate channel numbers for parameters where the system would be in the bistable regime in the deterministic limit ($N_K \rightarrow \infty$, see Appendix B). Hence, the wave solutions in the deterministic limit are fronts. However, as we showed before [33] to be in the bistable regime in the deterministic limit is not a necessary condition for backfiring to occur. Rather, backfiring occurs for parameters in the vicinity of a bifurcation separating the excitable from the bistable regime. In the excitable regime, the deterministic wave form are pulses.

For N_K smaller than the values for which backfiring occurs, abortive waves or steadily propagating pulses without backfiring were found. Reopening, obviously, is too unlikely to occur for small N_K .

VI. DISCUSSION

We have simulated spontaneous pattern formation of intracellular Ca^{2+} waves with a stochastic, discrete model using the DeYoung-Keizer-model of the IP_3 receptor channel. Our model reproduces the continuum of wave phenomena observed by Parker et al. [14], i.e. it shows a transition from isolated sparks to steady waves with increasing $[\text{P}_3]$. This transition was found for parameters of the channel kinetics suggested in the original paper by Keizer et al. introducing the IP_3R model.

We found a new state, which is characterized by backfiring. It provides for repetitive generation of waves without a pacemaker and explains the origin of waves observed in experiments even in regimes where spontaneous generation from the rest state is very unlikely to occur. Note, that the backfiring reported here is different from the backfiring in a deterministic model reported by Zimmermann et al. in [36]. There, backfiring occurs because the steadily propagating pulse solution undergoes a global heteroclinic bifurcation.

We found effects of stochasticity for numbers of channels per cluster as large as 250 (see Fig.8). That number allows for about maximal 50 open channels, which is at the upper limit of the number of open channels estimated from experiments. That shows, that the pattern

formation in biological cells is always in a regime where stochastic effects are relevant (like e.g. backfiring).

Our stochastic model shows pulses as wave solutions for parameters where the system would be in the bistable regime in the deterministic limit; i.e. cells might be in the bistable regime, even when pulses are observed. That supports theoretical and experimental findings for bistability in *Xenopus* oocytes with energized mitochondria [21].

We have shown, that the Ca^{2+} dynamics can be eliminated adiabatically. That means that the original system can be reduced to an array of stochastic, coupled elements the behavior of which is determined by 6 independent parameters only (e.g. $p_{0,1}^+$, p_0^- , p_d^\pm , N_K). We expect this reduction to hold for models including concentration dependent buffering, as long as the time scales of the buffer dynamics is faster than or similar to that of Ca^{2+} release, uptake and diffusion.

APPENDIX A: ANALYTIC SOLUTION OF THE PDE FOR CA^{2+} CONCENTRATION

Here, we briefly outline how the Ca^{2+} profiles for a single cluster with open channels in one and two spatial dimensions and the stationary solution for an array of clusters with identical numbers open channels in one spatial dimensions is obtained. In principle, analytic solutions could be derived for any configuration of open channels but would be quite tedious to calculate in general.

To solve equations(1,2) we apply a Laplace transformation to the time dependence of c, solve the resulting ODE's inside and outside the cluster with the initial condition $c(0, r) = C_s$ and obtain the equation for the mode time constant s from the boundary and matching conditions. In one spatial dimension we reach for a single cluster with N_o open channels and zero flux boundary conditions at $r=\pm L$:

$$c_{in}(s, r) = \frac{C_t}{s} - \frac{C_t \cosh(\nu_{in} r)}{\nu_{in} \sinh(\nu_{in} R) s F(s)} \quad (\text{A1})$$

$$c_{out}(s, r) = \frac{C_t \cosh(\nu_{out}(r - L))}{\nu_{out} \sinh(\nu_{out}(R - L)) s F(s)} \quad (\text{A2})$$

$$F(s) = \frac{\coth(\nu_{in} R)}{\nu_{in}} + \frac{\coth(\nu_{out}(R - L))}{\nu_{out}} \quad (\text{A3})$$

$$\nu_{in} = \sqrt{\frac{s + \frac{N_o J_T}{2RN_K}}{D}} \quad (\text{A4})$$

$$\nu_{out} = \sqrt{\frac{s + J_P + (1 + \alpha) J_L}{D}} \quad (\text{A5})$$

$$C_t = \frac{C_o}{1 + \alpha} - C_s \quad (\text{A6})$$

$$C_s = \frac{J_L C_o}{(1 + \alpha) J_L + J_P} \quad (\text{A7})$$

$$J_T = 2R(1 + \alpha) J_K \quad (\text{A8})$$

The solution of the same problem reads in two spatial dimensions:

$$c_{in}(s, r) = \frac{C_t}{s} + \frac{C_t \nu_{out} R I_0(\nu_{in} r / R)}{\nu_{in} I_1(\nu_{in}) s F(s)} \quad (\text{A9})$$

$$(K_1(\nu_{out} L) I_1(\nu_{out} R) - I_1(\nu_{out} L) K_1(\nu_{out} R))$$

$$c_{out}(s, r) = \frac{C_t (I_1(\nu_{out} L) K_0(\nu_{out} r) + K_1(\nu_{out} L) I_0(\nu_{out} r))}{s F(s)} \quad (\text{A10})$$

$$F(s) = I_1(\nu_{out} L) K_0(\nu_{out} R) + K_1(\nu_{out} L) I_0(\nu_{out} R) + \frac{\nu_{out} R I_0(\nu_{in})}{\nu_{in} I_1(\nu_{in})} (I_1(\nu_{out} L) K_1(\nu_{out} R) - K_1(\nu_{out} L) I_1(\nu_{out} R)) \quad (\text{A11})$$

$$\nu_{in} = \sqrt{\frac{s R^2 + \frac{N_o J_T}{N_K \pi}}{D}} \quad (\text{A12})$$

$$\nu_{out} = \sqrt{\frac{s + J_P + (1 + \alpha) J_L}{D}} \quad (\text{A13})$$

$$J_T = \pi R^2 (1 + \alpha) J_K \quad (\text{A14})$$

Modes are determined by the roots s_i of $sF(s) = 0$. In one spatial dimension, that leads to:

$$c_{in}(t, r) = C_t + C_s - \sum_{i=0}^{\infty} e^{s_i t} \frac{C_t \cosh(\nu_{in} r)}{\nu_{in} \sinh(\nu_{in} R) \left. \frac{dsF(s)}{ds} \right|_{s_i}} \quad (\text{A15})$$

$$c_{out}(t, r) = C_s + \sum_{i=0}^{\infty} e^{s_i t} \frac{C_t \cosh(\nu_{out}(r - L))}{\nu_{out} \sinh(\nu_{out}(R - L)) \left. \frac{dsF(s)}{ds} \right|_{s_i}} \quad (\text{A16})$$

and in two dimensions:

$$c_{in}(t, r) = C_t + C_s + \sum_{i=0}^{\infty} (K_1(\nu_{out} L) I_1(\nu_{out} R) - I_1(\nu_{out} L) K_1(\nu_{out} R)) e^{s_i t} \frac{C_t \nu_{out} R I_0(\nu_{in} r / R)}{\nu_{in} I_1(\nu_{in}) \left. \frac{dsF(s)}{ds} \right|_{s_i}} \quad (\text{A17})$$

$$c_{out}(t, r) = C_s + \sum_{i=0}^{\infty} e^{s_i t} \frac{C_t (I_1(\nu_{out} L) K_0(\nu_{out} r) + K_1(\nu_{out} L) I_0(\nu_{out} r))}{\left. \frac{dsF(s)}{ds} \right|_{s_i}} \quad (\text{A18})$$

In Fig.9 we compare the analytic solution (A17,A18) with simulations. Note that the stationary profile is reached essentially after 30ms.

The stationary solution of a one-dimensional periodic array of identical clusters with identical N_o^i is (with i being the position of the center of the i th cluster):

$$c_{in}(r) = C_t + C_s + \frac{C_t \nu_{out} (e^{\nu_{out} R} - e^{\nu_{out} (d-R)})}{B} \cosh(\nu_{in} (r - id)) \quad (\text{A19})$$

$$c_{out}(r) = C_s + \frac{C_t \nu_{in} \sinh(\nu_{out} R)}{B} (e^{\nu_{out} (r-id)} + e^{\nu_{out} (d-(r-id))}) \quad (\text{A20})$$

$$B = \nu_{in} \sinh(\nu_{in} R) (e^{\nu_{out} R} + e^{\nu_{out} (d-R)}) - \nu_{out} \cosh(\nu_{in} R) (e^{\nu_{out} R} - e^{\nu_{out} (d-R)}), \quad (\text{A21})$$

$$id \leq r \leq (i+1)d$$

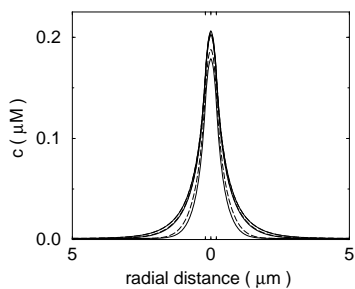


FIG. 9. Temporal evolution of the spatial Ca^{2+} profile for a single open cluster in 2 spatial dimensions. Simulation: full line, analytic solution dashed line. With increasing peak amplitude: $t=7.5\text{ms}$ (simulation), $t=7.5\text{ms}$ (analytic), $t=30\text{ms}$, $t=80\text{ms}$. For the two latter profiles the analytic solution and the simulation are undistinguishable. Simulation parameters: spatial discretization $0.0125\mu\text{m}$, time discretization 0.000125s , fully implicit scheme. Parameters not given in Table I are $J_P=46.87\mu\text{Ms}^{-1}$, $J_K=525\text{s}^{-1}$, $J_L=0.05\text{s}^{-1}$, $C_o=0.8\mu\text{M}$, $N_o=N_K=25$, $R=0.2125\mu\text{m}$.

APPENDIX B: STATIONARY, SPATIALLY PERIODIC SOLUTIONS OF THE COMPLETE MODEL IN THE DETERMINISTIC LIMIT

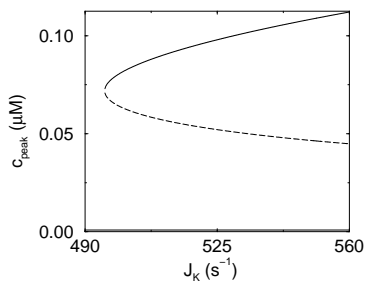


FIG. 10. Peak values of the Ca^{2+} concentration of the stationary, spatially periodic solutions of the complete model in the deterministic limit in dependence on J_K . Stable solutions: full lines, unstable solution: dashed line. Parameters not given in Table I are $d=1.5\mu\text{m}$, $J_P=52.5\mu\text{Ms}^{-1}$, $J_L=0.05\text{s}^{-1}$, $C_o=0.8\mu\text{M}$, $R=0.2\mu\text{m}$.

Equations (A19-A21) can be used to look for spatially periodic stationary solutions of the complete model in the deterministic limit, if N_o^i/N_K is determined as the fraction of open channels of the stationary solution. At small J_K , only one stationary solution exist. At the parameters used in this paper, N_o^i for the this stationary Ca^{2+} profile is so small, that deviations from the solution $N_o^i=0$ are negligible. Hence, this stationary solution is essentially $c(r,t)=C_s$. At higher values, two additional stationary solutions appear in a saddle node bifurcation and the system becomes bistable. We illustrate that in Fig. 10 by the peak values of the Ca^{2+} concentration in the center of the cluster. The solution with the higher peak value is stable, the one with intermediate peak values is unstable. A similar transition for the nonperiodic case of a single open cluster occurs at even higher values of J_K .

-
- [1] Alberts, B., D.Bray, J.Lewis, M.Raff, K.Roberts, J.D.Watson, 1994, Molecular Biology of the Cell, Garland Publishing, Inc. New York & London
 - [2] Kandel, E.R., J.H.Schwartz, T.M.Jessel, 1991, Principles of Neural Science, Appleton & Lange, Norwalk, Connecticut
 - [3] Ridgeway, E.B., J.C.Gilkey, L.F.Jaffe, 1977, Proc.Natl.Acad.Sci. USA 74:623
 - [4] Lechleiter, J., S.Girard, E.Peralta, D.Clapham, 1991, Science 252:123-129
 - [5] Fontanilla, R.A., R.Nuccitelli, 1998, Biophys.J. 75:2079-2087
 - [6] Nathanson, H.N., A.D.Burgstahler, M.B.Fallon, 1994, Am. J. Physiol. 267:G338-G349
 - [7] D'Andrea, P., F.Vittur, 1995, Biochemical and Biophysical Research Communications, 215:129-135
 - [8] Orchard, C.H., M.R.Mustafa, K.White, 1995, Chaos, Solitons & Fractals, 5:447-458
 - [9] Wussling, M.H.P., H.Salz, 1996, Biophys. J. 70:1144-1153
 - [10] Parker, I., Y.Yao, 1995, Calcium puffs in Xenopus oocytes, In calcium Waves, Gradients and Oscillations, G.R.Bock, K.Ackrill, editors, Wiley, Chichester, England
 - [11] Yao, Y., I.Parker, 1995, Journal of Physiology (Cambridge) 482.3:533-553
 - [12] Parker, I., Y.Yao, 1996, J.Physiol.(Lond.) 491:663-668
 - [13] Callamaras, N., J.S.Marchant, X.-P.Sun, I.Parker, 1998, Journal of Physiology 509.1:81-91
 - [14] Sun, X.-P., N.Callamaras, J.S.Marchant, I.Parker, 1998, Journal of Physiology 509.1:67-80

- [15] Schneider, M.F., M.G.Klein, 1996, Cell Calcium 20(2):123-128
- [16] Cheng, H., W.J.Lederer, M.B.Cannel, 1993, Am.J.Physiol. 270:C148-C159
- [17] Jafri, M.S., J.Keizer, 1995, Biophys.J. 69:2139-2153
- [18] Tang, Y., J.L.Stephenson, H.G.Othmer, 1996, Biophys. J. 70:246-263
- [19] Atri, A., J.Amundson, D.Clapham, J.Sneyd, 1993, Biophys. J., 65:1727-1739
- [20] Falcke, M., M.Bär, J.D.Lechleiter, J.L.Hudson, 1999, Physica D, 129.3-4:236-252
- [21] Falcke, M., J.L.Hudson, P.Camacho, J.D.Lechleiter, 1999, Biophys.J. 77:37-44
- [22] Jouaville, L.S., F.Ichas, E.L.Holmuhamedov, P.Camacho, J.D.Lechleiter, 1995, Nature 377:438-441
- [23] Sneyd, J., L.V.Kalachev, 1994, Cell Calcium 15.4:289-296
- [24] McKenzie, A., J.Sneyd, 1998, International Journal of Bifurcations and Chaos, 8.10:2003-2012
- [25] Wagner, J., Y.-X. Li, J.Pearson, J.Keizer, 1998, Biophys.J. 75:2088-2097
- [26] Mitkov, I., K.Kladko, J.E.Pearson, 1998, Phys.Rev.Lett. 81:5453-5456
- [27] Bugrim, A.E., A.M.Zhabotinsky, I.R.Epstein, 1997, Biophys.J. 73:2897-2906
- [28] Pearson, J.E., S.Ponce-Dawson, 1998, Physica A 257:141-148
- [29] Keizer, J., G.D.Smith, 1998, Biophys.Chem. 72:87-100
- [30] Keizer, J., G.D.Smith, S.Ponce-Dawson, J.E.Pearson, 1998, Biophys.J. 75:595-600
- [31] DeYoung, G.W., J.Keizer, 1992, Proc.Natl.Acad.Sci USA, 89:9895-9899
- [32] Keizer, J., G.DeYoung, 1994, J.theor.Biol., 166:431-442
- [33] M.Bär, M.Falcke, H.Levine, L.S.Tsimring, "Discrete stochastic modelling of calcium channel dynamics", submitted to Phys.Rev.Lett.
- [34] Wagner, J., J.Keizer, 1994, Biophys.J. 67:447-456
- [35] Sneyd, J., P.D.Dale, A.Duffy, 1998, SIAM J. on Applied Mathematics 58:1178-1192
- [36] M.G.Zimmermann, S.O.Firle, M.A.Natiello, M.Hildebrand, M.Eiswirth, M.Bär, A.K.Bangia, I.G.Kevrekidis, 1997, Physica D 110:92-104